Soft Matter

Accepted Manuscript

This article can be cited before page numbers have been issued, to do this please use: J. Clopes, G. Gompper and R. G. Winkler, *Soft Matter*, 2020, DOI: 10.1039/D0SM01569E.

ROYAL SOCIETY OF CHEMISTRY

rsc.li/soft-matter-journal

View Article Online
DOI: 10.1039/D0SM01569E

Cite this: DOI: 10.1039/xxxxxxxxxx

Received Date
Accepted Date

DOI: 10.1039/xxxxxxxxxx

www.rsc.org/journalname

Hydrodynamic interactions in squirmer dumbbells: active stress-induced alignment and locomotion

Judit Clopés, Gerhard Gompper, and Roland G. Winkler

Hydrodynamic interactions are fundamental for the dynamics of swimming self-propelled particles. Specifically, bonds between microswimmers enforce permanent spatial proximity and, thus, enhance emergent correlations by microswimmer-specific flow fields. We employ the squirmer model to study the swimming behavior of microswimmer dumbbells by mesoscale hydrodynamic simulations, where the squirmers' rotational motion is geometrically unrestricted. An important aspect of the applied particle-based simulation approach—the multiparticle collision dynamics method—is the intrinsic account for thermal fluctuations. We find a strong effect of active stress on the motility of dumbbells. In particular, pairs of strong pullers exhibit orders of magnitude smaller swimming efficiency than pairs of pushers. This is a consequence of the inherent thermal fluctuations in combination with the strong coupling of the squirmers' rotational motion, which implies non-exponentially decaying auto- and cross-correlation functions of the propulsion directions, and active stress-dependent characteristic decay times. As a consequence, specific stationary-state relative alignments of the squirmer propulsion directions emerge, where pullers are preferentially aligned in an antiparallel manner along the bond vector, whereas pushers are preferentially aligned normal to the bond vector with a relative angle of approximately 60° at weak active stress, and one of the propulsion directions is aligned with the bond at strong active stress. The distinct differences between dumbbells comprised of pusher or pullers suggest means to control microswimmer assemblies for future microbot applications.

1 Introduction

Active matter consists of autonomous agents which convert internal chemical energy or environmental energy into directed motion[1–5]. Characteristic features of active matter are broken time-reversal symmetry, broken detailed balance, and absence of a fluctuation-dissipation relation. This gives rise to phenomena, which are absent in passive counterparts, such as enhanced wall accumulation[6–10], and cooperative[11] and large-scale collective motion[12–19]. Active matter-specific effects provide the basis for, and can be exploited in, the design of new functional soft materials[20–23].

Theoretically, various models and approaches are applied to resolve the particular features of active matter systems. The paradigmatic model for dry active matter agents—absence of hydrodynamic interactions—are Active Brownian Particles (ABPs)[1–4,24–28]. Ensembles of this generic model capture basic features of active systems, such as motility-induced phase separation (MIPS)[3,4,24–26,29–35], where the high density phase in two dimensions (2D) exhibits hexatic order[32], whereas in 3D, ABPs are fluid-like and are highly mobile even in the high-density regime, and exhibit collective motion[33].

Linear assemblies of freely rotating ABPs, where the orientational degrees of freedom are unconstrained, in form of dumbbells[36,37] and longer chains[22,23,38–44] have been studied. Here, the coupling of activity and internal degrees of freedom strongly affects their conformations and dynamics. Alternatively, active dumbbells propelled along the bond connecting the two monomers are considered[45,46]. Here, dumbbell rotation is independent of activity and a consequence of thermal fluctuations only[47]. Moreover, fixation of the orientation between the propulsion directions of the two monomers with respect to each other and/or the bond vector, provides a wide spectrum of possible realizations. As an example, the phase behavior of dumbbells with fixed parallel propulsion directions undergoing Brownian motion has been studied[37]. Experiments show that dumbbells of Janus-particle monomers with a fixed non-parallel relative orientation exhibit a coupled translational and rotational motion. Hence, such structures provide means for the design of swimmers moving along specific trajectories[48,49] such as spirals[49]. Simula-

Theoretical Physics of Living Matter, Institute of Biological Information Processing and Institute for Advanced Simulation, Forschungszentrum Jülich and JARA, D-52425 Jülich, Germany
Email: g.gompper@fz-juelich.de, r.winkler@fz-juelich.de

View Article Online
DOI: 10.1039/D0SM01569E

tions reveal a strong influence of the propulsion mechanism on the activity-induced phase separation of dumbbells. For example, dumbbells propelled along the bond in 2D phase separate at smaller activities than ABPs[50]. In contrast, dumbbells of freely rotating ABPs phase separate at larger activities[37]. Hence, depending on the orientation of the propulsion directions and their correlations, the phase behavior can be controlled.

A generic model for wet active particles—hydrodynamic interactions are present[28]—are squirmers[11,51–57], originally intended to model ciliates and microalgae. Nowadays, squirmers are applied in studies of a broad range of both biological[58] and synthetic microswimmers[59], because squirmers can be tuned to capture essential features of microswimmers flow fields—from pushers (*E. coli*) to ciliates (*Volvox*) and pullers (*Chlamydomonas reinhardtii*)[60]. Studies on spherical squirmers in presence and absence of thermal fluctuations reveal attractive and repulsive interactions at distances larger than their diameter[11,53,55,56,61]. Remarkably, the hydrodynamic interactions between spherical squirmers[60], and microswimmer in general[62], suppresses MIPS and can lead to particular ordered structures in absence of thermal fluctuations[63,64].

So far, very little is known about the effect of the microswimmer flow field on the properties of dumbbells composed of two squirmers, which are permanently linked by a bond. Theoretical studies on the athermal case show specific swimming behaviors different from those of dry active dumbbells[65]. In particular, no stable forward swimming can be achieved within a far-field consideration of freely rotating, torque-free swimmers. A restriction of the rotational motion of the individual squirmers by (rigid) bonds leads to torques and stable swimming motion for various dumbbell arrangements and pusher-puller combinations[65]. Thermal fluctuations can be expected to destabilize the predicted stationary states and to imply a yet unexplored swimming behavior, which is naturally absent in dry ABP-type systems.

The combination of squirmers into dumbbells is particularly interesting, since it is a minimal model of linked microswimmers, and forms the basis for autonomous units, e.g., linear polymers or more complex assemblies, as a possible prerequisite of autonomous microbots. Even more, the phase behavior of dumbbell ensembles is determined by interactions via the flow field of the microswimmers to an extent unexplored so far, but can be expected to be different from that of dry ABP dumbbell ensembles.

In this article, we study the properties of freely rotating squirmers linked by a bond of finite length embedded in a fluid. We apply the multiparticle collision dynamics approach (MPC) to model the fluid, a particle-based mesoscale simulation approach, which accounts for hydrodynamic interactions and thermal fluctuations[58,66,67]. MPC has successfully been utilized in studies of a broad range of nonequilibrium soft matter and active systems, in particular applying squirmers[11,55,60,68–74]. The presence of thermal fluctuations fundamentally alters the swimming properties of dumbbells compared to athermal ones. Most importantly, the fluctuations imply a rotational diffusive motion of the individual squirmers, and the dumbbells are able to swim in contrast to the athermal case[65]. Our detailed analysis of the squirmers' rotational motion reveals a pronounced dependence on their particular flow field, with the decay rate of autocorrelation function of the propulsion direction strongly depending on the active stress. This affects the dumbbells' swimming motion, with major differences in the dumbbell center-of-mass mean-square displacement, specifically between pusher and puller dumbbells. In particular, the squirmers' propulsion directions are no longer independent, but rather are correlated with preferred activity-dependent angles between them in the stationary state.

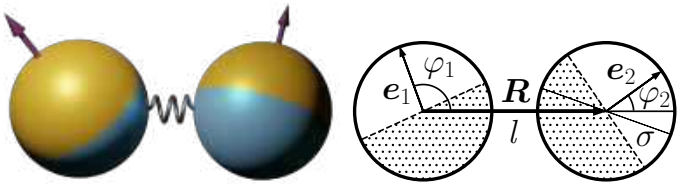

Fig. 1 Schematics of a squirmer dumbbell with squirmers of diameter σ, bond vector $\boldsymbol{R}$, and propulsion directions $\boldsymbol{e}_1$ and $\boldsymbol{e}_2$. The colors of the semispheres indicate the propulsion asymmetry.

This article is structured as follows. In Sec.2, the simulation approach is introduced with the squirmer dumbbell model and its coupling to the MPC fluid. Section 3 presents results on the orientational dynamics of the squirmers and the swimming behavior of dumbbells. In Sec. 4, the stationary-state orientational properties of the squirmer propulsion directions with respect to each other and the dumbbell bond vector are analyzed. Finally, Sec. 6 provides a summary of the results.

2 Simulation approach

2.1 Dumbbell model

The active dumbbell is composed of two freely rotating spherical squirmers as shown schematically in Fig. 1. An individual squirmer is modeled as a rigid sphere of diameter σ with the prescribed tangential slip velocity on its surface,

$$\boldsymbol{u}_{\mathrm{sq}} = B_1 \sin\theta(1+\beta\cos\theta)\boldsymbol{e}_\theta, \tag{1}$$

which generates propulsion with a velocity $v_0 = 2B_1/3$ and an active stress characterized by β[11,28,51–53,55,56,61,72,75]. The sign of the active stress determines the squirmers' swimming mechanisms—for pullers (*C. reinhardtii*) $\beta > 0$ and the thrust mechanism is at the front, for pushers (*E. coli*) $\beta < 0$ and thrust is produced in the rear of the swimmer. The value $\beta = 0$, for neutral squirmers, corresponds to ciliates such as *Volvox* or *Paramecia*[28,71]. The corresponding flow fields of individual squirmers are discussed in Ref.[27,71], and Fig. 2 provides examples of dumbbell flow fields for various active stresses β[23].

The two squirmers at positions $\boldsymbol{r}_1$ and $\boldsymbol{r}_2$ are connected by the harmonic potential

$$U_l = \frac{k}{2}(|\boldsymbol{R}| - l)^2, \tag{2}$$

with the bond vector $\boldsymbol{R} = \boldsymbol{r}_2 - \boldsymbol{r}_1$, the equilibrium bond length l, and the spring constant k. The squirmer orientations $\boldsymbol{e}_i$, $|\boldsymbol{e}_i| = 1$, $i \in \{1, 2\}$, change in response to thermal fluctuations and hydrodynamic interactions by their flow fields.

View Article Online
DOI: 10.1039/D0SM01569E

To quantify activity, we introduce the Péclet number[3,34,36,76]

$$\mathrm{Pe} = \frac{v_0}{\sigma D_R^0}, \tag{3}$$

where D_R^0 is the rotational diffusion coefficient of an individual squirmer in a three dimensional dilute solution, and v_0 its swim velocity.

2.2 Fluid model: Multiparticle collision dynamics (MPC)

In MPC, the fluid is described as an ensemble of N point particles of mass m. Their dynamics proceeds in two alternating steps: streaming and collisions, updating the particle positions $\boldsymbol{r}_i$ and velocities $\boldsymbol{v}_i$ ($i \in \{1,\ldots,N\}$). In the streaming step, MPC particles move ballistically during a collision time h and their positions are updated as

$$\boldsymbol{r}_i(t+h) = \boldsymbol{r}_i(t) + h\boldsymbol{v}_i(t). \tag{4}$$

Momentum exchange between particles takes place in the collision step. Here, the particles are sorted into cubic cells of mesh size a defining the local interaction environment. The velocities of the fluid particles after a collision, $\boldsymbol{v}_i(t+h)$, are given by[77,78]

$$\begin{aligned}\boldsymbol{v}_i(t+h) &= \boldsymbol{v}_{\mathrm{cm}}(t) + \mathbf{R}(\alpha)\boldsymbol{v}_{i,\mathrm{cm}}(t) \\ &- \boldsymbol{r}_{i,\mathrm{cm}} \times \left[m\mathbf{I}^{-1} \sum_{j\in\mathrm{cell}} \boldsymbol{r}_{j,\mathrm{cm}} \times (\boldsymbol{r}_{j,\mathrm{cm}} - \mathbf{R}(\alpha)\boldsymbol{v}_{j,\mathrm{cm}}) \right],\end{aligned} \tag{5}$$

within the stochastic-rotation-dynamics (SRD) variant with angular momentum conservation of MPC (MPC-SRD+a)[11,77]. In Eq. (5), $\mathbf{R}(\alpha)$ is the rotation matrix for the rotation of the relative velocity $\boldsymbol{v}_{i,\mathrm{cm}} = \boldsymbol{v}_i - \boldsymbol{v}_{\mathrm{cm}}$ with respect to the center-of-mass velocity $\boldsymbol{v}_{\mathrm{cm}}$ of the cell of particle i by a fixed angle α around a randomly oriented axis[79]. $\mathbf{I}$ is the inertia tensor in the cell's center-of-mass reference frame and $\boldsymbol{r}_{i,\mathrm{cm}} = \boldsymbol{r}_i - \boldsymbol{r}_{\mathrm{cm}}$ is the difference vector with respect to the center-of-mass position $\boldsymbol{r}_{\mathrm{cm}}$ of the cell of particle i. A constant temperature is maintained by applying the cell-level canonical Maxwell-Boltzmann scaling (MBS) thermostat after every collision step[79]. The MPC algorithm is highly parallel, hence, a graphics processor unit (GPU)-based version for a high performance gain is employed[80] (see ESM).

2.3 Implementing squirmers in MPC

A squirmer is a neutrally buoyant rigid spherical colloidal particle of mass M, diameter σ, center-of-mass position $\boldsymbol{C}$, orientation $\boldsymbol{e}$, translational velocity $\boldsymbol{v}$, and angular momentum $\boldsymbol{L}$. During the MPC streaming step, it moves according to the rigid-body dynamics, where the rotational motion is described by quaternions[11,81]. Interactions with MPC particles lead to changes of the linear and angular momentum of a squirmer (cf. ESM). In the MPC collision step, phantom particles are uniformly distributed inside each colloid, which take part in the MPC collisions and improve the no-slip boundary condition[11,82,83]. Their number density and mass are equal to those of fluid particles. MPC collisions lead to a change of the phantom particles moments, which are transferred to the colloid and change its linear and angular momentum[11]. Details of the algorithm and the interactions of a squirmer with MPC particles are described in the ESM.

2.4 Parameters

Dumbbells are composed of squirmers of diameter $\sigma = 6a$, mass $M = 10m$, bond length $l = 8a$, and $k = 5000\ k_BT/(ma^2)$, where k_B is the Boltzmann constant and T the temperature. The rigid-body equations of motion are solved with the time step $\Delta t = 0.002\sqrt{ma^2/(k_BT)}$. For the MPC fluid, we use the mean number of particles per collision cell $\langle N_c\rangle = 10$, the rotation angle $\alpha = 130°$, and the collision step size $h = 0.05\sqrt{ma^2/(k_BT)}$, which yields the fluid viscosity $\eta \approx 7.2\sqrt{mk_BT/a^4}$. The latter value is approximately 10% smaller than the theoretical value $\eta_t = 8.1\sqrt{mk_BT/a^4}$, consistent with previous studies[78]. Simulations yield the rotational diffusion coefficient $D_R^0 = 2.2\times10^{-4}\sqrt{k_BT/(ma^2)}$ of a passive colloid in dilute solution. The length of the simulation box is $L = 40a$. Displayed results are averages over at least 10 independent realizations for every parameter set.

We consider the values $B_1/\sqrt{k_BT/m} = 0.02 - 0.12$, which correspond to the Péclet numbers $\mathrm{Pe} = 10 - 60$ (Eq. (3)) and the Reynolds numbers $\mathrm{Re} = v_0\sigma/\nu = 0.12 - 0.72 < 1$ for the considered squirmer size and MPC fluid parameters, where $\nu = \eta/(m\langle N_c\rangle/a^3)$ is the kinematic viscosity. Since the swimming velocity of the dumbbell depends on the active stress and can be substantially smaller than v_0, cf. Sec. 5.2, these Reynolds numbers are an upper limit for the respective B_1 (v_0) value; for example, $Re < 0.05$ for $\beta \gtrsim 1$.

Moreover, the oscillatory Reynolds number Re_T is finite, where Re_T is the ratio of the viscous time scale τ_ν for shear-wave propagation over a characteristic length scale and a characteristic time scale (frequency) of the dumbbell[84,85]. Here, we set $\tau_\nu = l^2/\nu$ and the relevant time scale is given by the rotational motion of a squirmer, hence, $\mathrm{Re}_T = 2D_Rl^2/\nu$. The above parameters yield $Re_T = 0.04$ for $D_R = D_R^0$. Hence, rotation is sufficiently slow to ensure hydrodynamic coupling of the rotational motion of the two squirmers of a dumbbell.

3 Swimming behavior of freely jointed squirmer dumbbells

3.1 Dynamics of individual squirmers

The autocorrelation function $\langle \boldsymbol{e}(t)\cdot\boldsymbol{e}(0)\rangle$ of the rotational diffusive motion of passive colloids in a dilute suspension decays exponentially as

$$\langle \boldsymbol{e}(t)\cdot\boldsymbol{e}(0)\rangle = e^{-2D_R^0 t} \tag{6}$$

due to thermal fluctuations[86,87]. Similarly, the correlation function of individual squirmers embedded in a MPC fluid decays exponentially with the rotational diffusion coefficient D_R^0, since the rotational motion is independent of the active process and is only affected by thermal fluctuations in the fluid[11]. Moreover, the mean-square displacement of individual squirmers is independent of the active stress (β). Hence, the squirmer dynamics in dilute solution is characterized by the propulsion velocity v_0 and the rotational diffusion coefficient D_R^0 and is quantitatively described by an ABP with the same v_0 and D_R^0.

View Article Online
DOI: 10.1039/D0SM01569E

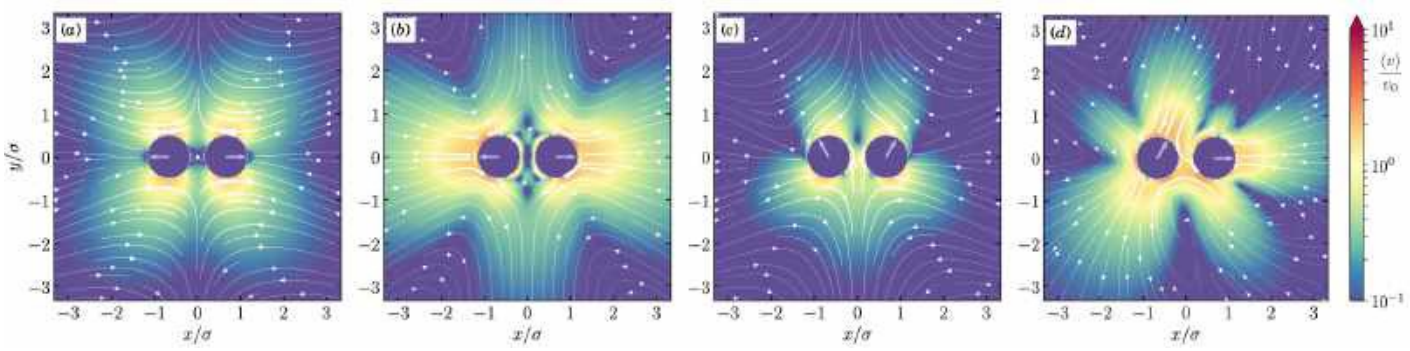

Fig. 2 Flow fields in the laboratory reference frame of most probable squirmer-squirmer relative orientations for different active stresses, β. For (a) neutral ($\beta = 0$) and (b) pullers ($\beta = 5$), the squirmers' propulsion directions point outward with respect to the center of the dumbbell. For (c) weak pushers ($\beta = -1$), there is a finite angle between the propulsion directions, both pointing "normal" to the dumbbell bond vector. In addition to the configuration in (c), (d) strong pushers ($\beta = -5$) exhibit states, where one of the propulsion directions is preferentially aligned with the bond vector. The flow fields have been obtained by a superposition of the two individual squirmer flow fields and their Stokeslets emerging from the bond force. The latter give rise to a force dipole. (Cf. ESM for movies).

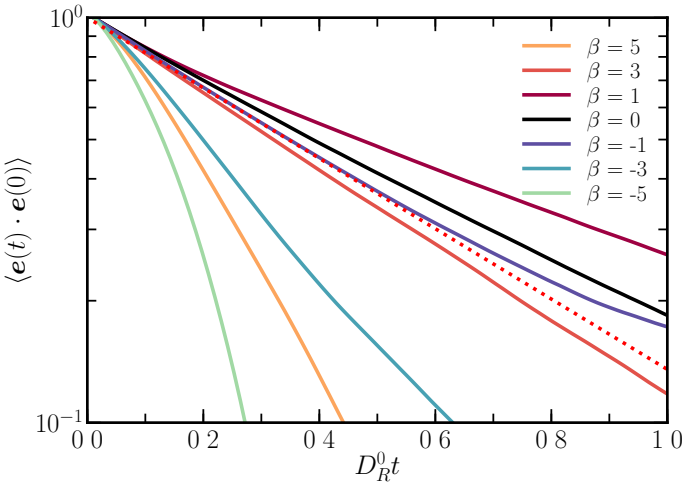

Fig. 3 Autocorrelation function of the squirmer propulsion direction as a function of the scaled time $D_R^0 t$, where D_R^0 is the rotational diffusion coefficient of a passive colloid (and independent squirmers), for $\mathrm{Pe} = 30$ and various active stresses as indicated in the figure. The red dotted line indicates the exponential decay of the correlation function a passive colloid with $D_R^0 = 2.2 \times 10^{-4}\sqrt{k_B T/(m a^2)}$.

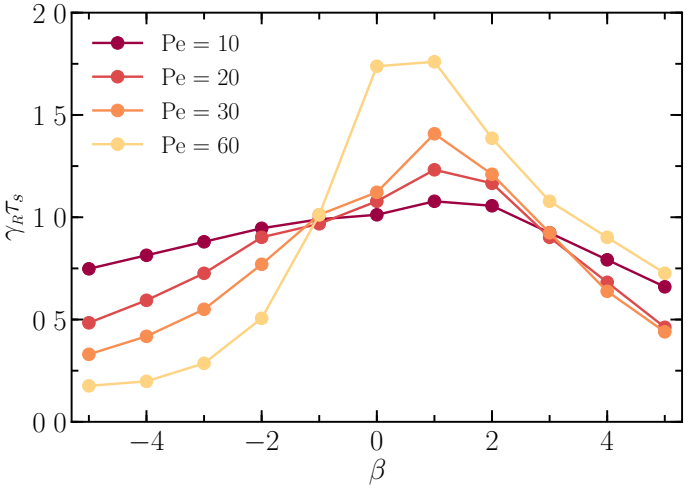

Fig. 4 Characteristic decay time τ_s of the autocorrelation function of Fig. 3 as a function of the active stress β for the Péclet numbers $\mathrm{Pe} = 10,\ 20,\ 30$, and 60. The decay time is scaled by the rotational diffusion coefficient of a passive colloid, where $\gamma_R = 2D_R^0$.

3.2 Squirmer rotational dynamics in a dumbbell

As for individual squirmers, the thermal fluctuations in a fluid imply a rotational motion of the squirmers in a dumbbell. This is in contrast to studies on athermal squirmers, where orientational changes occur by the interference of the flow fields of microswimmers only. As a consequence, for athermal dumbbells the squirmer orientations are fixed in the stationary state. This implies particular ordered structures in dense systems of individual athermal squirmers[63,64]. However, thermal fluctuations are an integral part in systems of biological and synthetic microswimmers and affect their rotational motion[4,88,89].

The decay of the autocorrelation of the propulsion direction, as shown in Fig. 3, is a function of the active stress β and may no longer decay by a single-exponential function due to the combined effect of thermal fluctuations and hydrodynamic interactions. To characterize the decay of the correlation function, we determine a characteristic time τ_s by the condition that the correlation function has decayed to $1/e$ at $t = \tau_s$. The decay time τ_s is presented in Fig. 4, reflecting a strong dependence on β and Pe. In the range $-5 < \beta < 1$, the decay time, τ_s, increases monotonically with β, and decreases nearly linearly for $1 < \beta < 5$. The range of τ_s values increases with increasing Pe. Interestingly, all pullers ($\beta > 0$) exhibit similar τ_s values in the range $20 < \mathrm{Pe} < 30$. Moreover, the decay-time curves for the various Pe all intersect at $\beta \approx -1$, indicating a Pe-independent relaxation. In the range $-1 < \beta \lesssim 3$, the orientational relaxation is slower than that of an individual, unbound squirmer, and larger Pe lead to longer relaxation times. For $\beta < -1$, τ_s decreases with increasing Pe, corresponding to a faster relaxation.

The spectrum of decay times and the difference with respect to the time $(2D_R^0)^{-1}$ of individual squirmers reveals the strong influence of the overlapping squirmer flow fields in a dumbbell on the squirmer dynamics. Naturally, this is distinctly different from the

View Article Online
DOI: 10.1039/D0SM01569E

behavior of ABP dumbbells, although pushers with $\beta = -1$ exhibit a very similar relaxation behavior. The hydrodynamic interplay is rather complex due to both, the reorientation dynamics of the individual squirmers and the rotation of linked squirmers around each other. Note that the bond is not restricting their individual solid-body rotation. This is also reflected in the correlation function of the propulsion directions with respect to the bond vector (cf. Figs. S2).

3.3 Crosscorrelation function of propulsion directions

The crosscorrelation function $\langle \boldsymbol{e}_1(t) \cdot \boldsymbol{e}_2(0) \rangle$ between the propulsion directions of the two squirmers, displayed in Fig. 5, illustrates their tight dynamical coupling, with functions decaying typically in a non-single exponential manner. Figure 6 depicts the characteristic decay time τ_c as a function of β for various Pe, which is defined in the same way as τ_s. In contrast to τ_s of individual squirmers in a dumbbell, τ_c decreases with increasing Pe for all β. The decay time increases monotonically with increasing β for pushers ($\beta < 0$) and decreases monotonically for pullers ($\beta > 0$), with a maximum for neutral squirmers ($\beta = 0$). Noteworthy, the τ_c values are always larger than the τ_s, i.e., the crosscorrelation function decays slower the autocorrelation function of a squirmer, which emphasizes the hydrodynamic coupling of the squirmer propulsion directions.

3.4 Bond-vector autocorrelation function

The bond-vector autocorrelation function of a flexible dumbbell of ABPs is given by[36]

$$\langle \boldsymbol{R}(t) \cdot \boldsymbol{R}(0) \rangle = l^2 e^{-t/\tau_l} + \frac{2v_0^2 \tau_l^2}{1-(\gamma_R \tau_l)^2} \left(e^{-\gamma_R t} - e^{-t/\tau_l} \right), \qquad (7)$$

with an activity-dependent relaxation time τ_l and γ_R. In the limit of vanishing activity ($v_0 \to 0$), the correlation function reduces to

$$\langle \boldsymbol{R}(t) \cdot \boldsymbol{R}(0) \rangle = l^2 e^{-t/\tau_l^0}, \qquad (8)$$

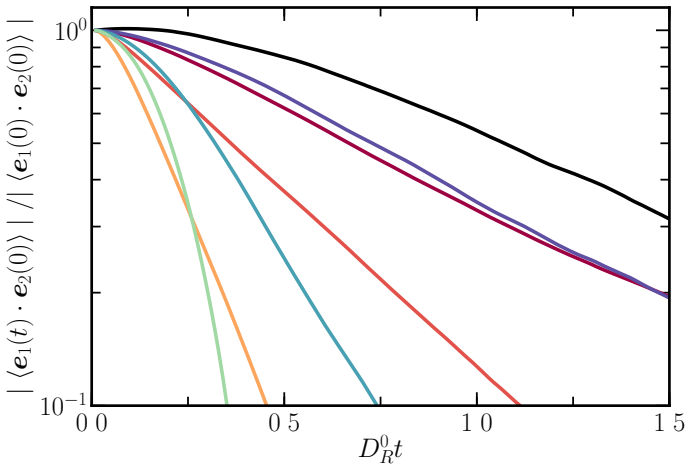

Fig. 5 Crosscorrelation function, $\langle \boldsymbol{e}_1(t) \cdot \boldsymbol{e}_2(0) \rangle$, of the squirmer orientations as a function of the scaled time $D_R^0 t$ for Pe = 30 and various active stresses β as indicated in the figure.

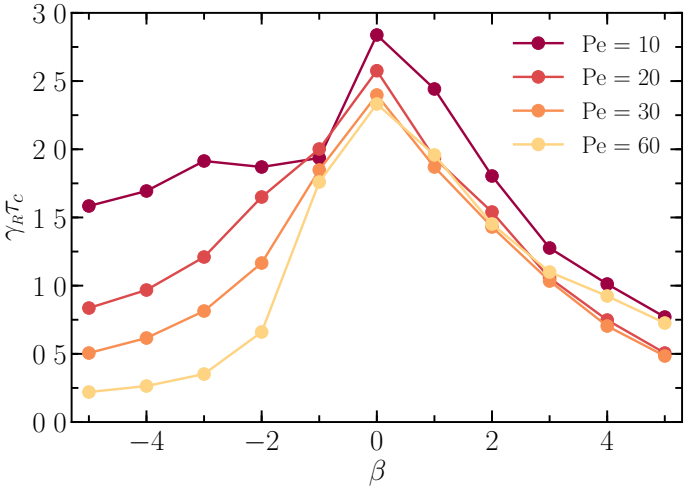

Fig. 6 Characteristic decay time τ_c of the crosscorrelation function of Fig. 5 as a function of the active stress β for the Péclet numbers Pe = 10, 20, 30, and 60. The decay time is scaled by the rotational diffusion coefficient of a passive colloid, where $\gamma_R = 2D_R^0$.

with the relaxation time $\tau_l^0 = \gamma_T l^2/(6k_BT)$, where γ_T is the translational friction coefficient of an individual colloid. Here, the decay of the correlation function is determined by the rotational diffusion of the dumbbell with the rotational diffusion coefficient $D_R^l = 3k_BT/(\gamma_T l^2)$[47] (cf. comment in Ref. 90). At high Péclet numbers, Eq. (7) becomes

$$\langle \boldsymbol{R}(t) \cdot \boldsymbol{R}(0) \rangle = l^2 e^{-2D_R t}, \qquad (9)$$

and the decay of the correlation function is governed by the rotational diffusion of the individual ABPs. In general, both relaxation processes contribute to the decay of the correlation function.

The squirmer dumbbell bond-vector autocorrelation function is depicted in Fig. 7 for Pe = 30. As for ABP dumbbells, the correlation function decays non-exponentially at short times. Neutral-squirmer and weak-puller ($\beta < 2$) dumbbells show a slower decay compared to an ABP dumbbell, which translates into a higher effective rotation diffusion coefficient D_R^l. For other active stresses, a faster decay than that of ABP dumbbells is obtained. Furthermore, the coupling of strong pushers results in a non-exponential decay of the bond-vector autocorrelation function, with negative correlations at intermediate times (Fig. 7), which indicates a particular dynamical behavior—a rotational motion of the whole dumbbell—as discussed in more detail in Sec. 4.2. The dependence of the decay times, τ_l, on β and Pe is qualitatively similar to that of τ_s as shown in Fig. S1.

4 Stationary-State Squirmer Propulsion Alignment

The strong interference of the squirmer flow fields combined with the Stokeslets emerging from the bond force implies particular average stationary state alignments of their propulsion directions with respect to each other and the bond vector.

View Article Online
DOI: 10.1039/D0SM01569E

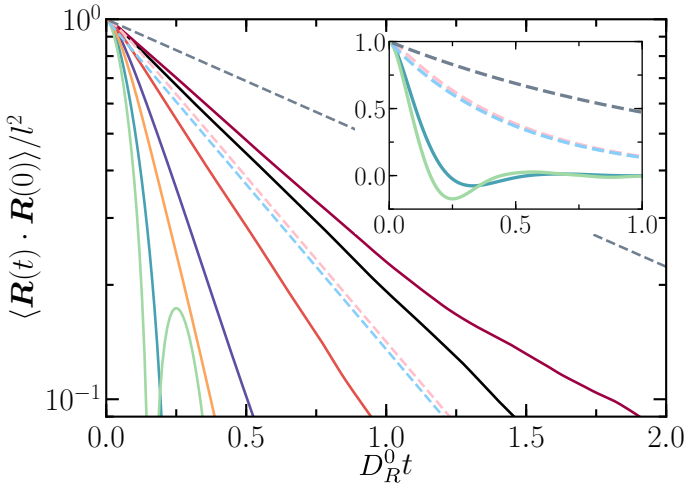

Fig. 7 Bond-vector autocorrelation function as a function of to the scaled time $D_R^0 t$ for $\mathrm{Pe} = 30$. The color code is the same as in Fig. 5. The light red dashed line is the bond-vector autocorrelation function for an ABP dumbbell (Eq. (7)). The gray and light blue lines are the limits $\mathrm{Pe} \to 0$ and $\mathrm{Pe} \to \infty$ described in Eq. (8) and (9), respectively. The inset shows the same data on linear scales.

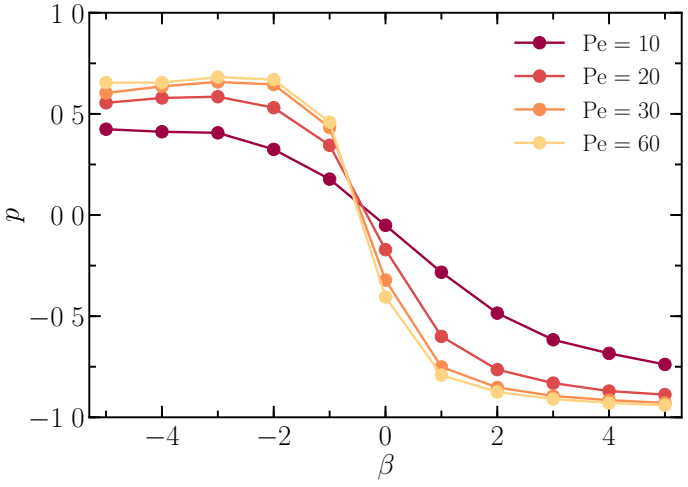

Fig. 8 Average alignment $p = \langle \boldsymbol{e}_1 \cdot \boldsymbol{e}_2 \rangle$ of the squirmer propulsion directions as a function of the active stress β for the Péclet numbers $\mathrm{Pe} = 10,\ 20,\ 30$, and 60 (bottom to top at $\beta = -5$).

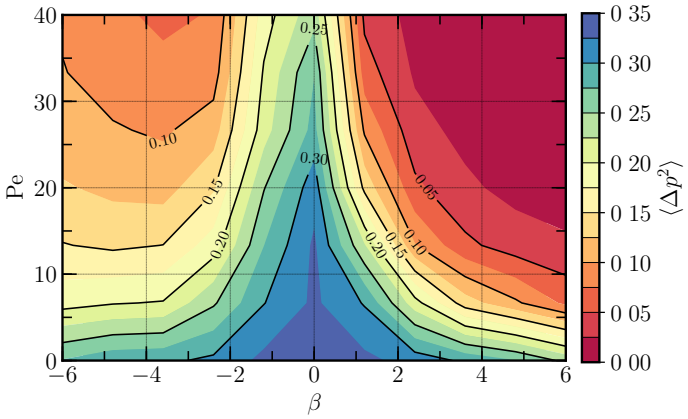

Fig. 9 Variance Δp^2 of the squirmers' alignment distribution function as a function of the active stress β and the Péclet number Pe.

4.1 Squirmer-squirmer propulsion alignment

The average cosine of the angle ϑ between the two propulsion directions,

$$p = \langle \boldsymbol{e}_1 \cdot \boldsymbol{e}_2 \rangle = \langle \cos \vartheta \rangle \,, \tag{10}$$

is displayed in Fig. 8. It changes nearly monotonically from a positive value for $\beta < 0$ to a negative value for $\beta > 0$, with a change of the angle from $\vartheta \approx 65^\circ$ to $\vartheta \approx 160^\circ$. An increasing activity amplifies the preference in alignment, and an asymptotic curve seems to be approached for large Pe. Interestingly, the asymptotic value for $\beta < -2$, $p \approx 0.65$, is far from a parallel as well as an orthogonal alignment. In contrast, pullers for $\beta > 2$ are almost aligned in an antiparallel manner with $p \approx -0.95$. Noteworthy, p for neutral squirmers is negative, corresponding to a preferred antiparallel alignment, and the curves for the various Pe intersect at $\beta \approx -0.5$, with an angle of $\vartheta \approx 90^\circ$. The preference for an outward antiparallel alignment is explained by the instability of conformations where $\pi/2 > \varphi_1 > -\pi/2$ and $\pi/2 < \varphi_2 < 3\pi/2$, i.e., already for a slight inward antiparallel alignment of the propulsion directions, where the whole dumbbell starts to rotate until the squirmer propulsion directions point antiparallely apart from each other.

Qualitatively, the observed alignment for pushers ($\beta < 0$) and pullers ($\beta > 0$) can be understood by the interactions between two force-dipoles[6,53,71,91], which yields parallel side-by-side arrangement of pushers and collinear alignment of pullers. The finite opening angle of $\vartheta \approx 65^\circ$ for pushers is a consequence of higher-order multipoles of the squirmer flow field[71]. This is reflected in diverging trajectories of side-by-side swimming pushers[53,55]. Similarly, the opposite orientation of the puller propulsion direction is due to higher-order multipoles.

The strong opposite alignment of pullers is consistent with the stable fixed point obtained for athermal squirmers within the far-field approximation[65]. To which extend near-field hydrodynamic effects are important remains to be analyzed.

Qualitatively different from the theoretical prediction for athermal dumbbells is the behavior of pusher dumbbells for $\beta < -1$. Due to thermal fluctuations and possibly near-field hydrodynamic effects, the preferred alignment angle, $\vartheta \approx 65^\circ$, is substantially different from the analytical derived values[65].

The stability of the squirmer alignment strongly depends on Pe and β. Figure 9 depicts the variance

$$\Delta p^2 = \langle (\boldsymbol{e}_1 \cdot \boldsymbol{e}_2)^2 \rangle - p^2 \tag{11}$$

of the squirmers' alignment distribution function. The fluctuations are extremely small for pullers at $\mathrm{Pe} \gtrsim 20$ and $\beta \gtrsim 3$, indicating a very strong preference in alignment. They are more than twice as large for $\beta \lesssim -2$ at $\mathrm{Pe} \gtrsim 25$, but still small. However, Δp^2 is large for $\beta \approx 0$ for all Péclet numbers.

4.2 Squirmer-propulsion bond alignment

To characterize the alignment of the squirmer propulsion direction relative to the dumbbell bond vector, $\boldsymbol{R}$, we consider the

View Article Online
DOI: 10.1039/D0SM01569E

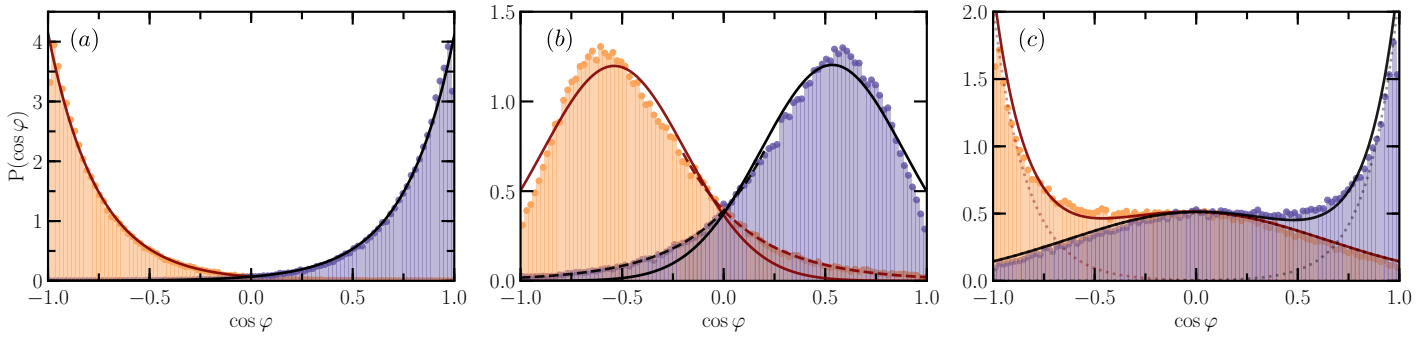

Fig. 10 Probability distribution function of the alignment of the squirmer propulsion direction with respect to the dumbbell bond vector, $\boldsymbol{e}_i \cdot \boldsymbol{R}/|\boldsymbol{R}| = \cos\varphi_i$, for each squirmer ($i = 1$, orange, $i = 2$ purple) and (a) $\beta = 0$, (b) $\beta = -1$, and (c) $\beta = -5$. The Péclet number is $\mathrm{Pe} = 30$. The solid lines are fits of (a) exponential and (b) Gaussian functions, respectively. In (b), dashed lines indicate exponential fits, and in (c), dotted lines Gaussian fits; the solid lines are the sum over the fit functions.

quantity

$$q_i = \frac{\boldsymbol{e}_i \cdot \boldsymbol{R}}{|\boldsymbol{R}|} = \cos\varphi_i. \tag{12}$$

Figure 10 displays the probability distribution function (PDF) of q_i for various $\beta \leq 0$. The PDFs for neutral squirmers decay exponentially with maxima at $\cos\varphi = \pm 1$, corresponding to a preferred antiparallel alignment of the propulsion directions. The distribution functions for pushers with $\beta = -1$ are approximately Gaussian (Fig. 10(b)), but with exponential tails, and exhibit maxima at $\varphi_1 \approx 127^\circ$ ($q_1 = -0.6$) and $\varphi_2 \approx 53^\circ$ ($q_2 = 0.6$), respectively, with respect to the bond vector (Fig. 2(c)). Such dumbbells preferentially swim in the direction normal to the bond vector. At $\beta = -5$, the q_i exhibit a preference for antiparallel/parallel alignment with respect to the bond vector. In addition, a broad plateau-like regime is present for $-1/2 < q_1 < 0$ and $0 < q_2 < 1/2$, respectively (Fig. 10(b)). The distribution functions can be considered as a superposition of two Gaussians, a narrow Gaussian for the antiparallel/parallel alignment with the bond, and a wide Gaussian for the broad spectrum of possible alignments with respect to the bond. However, typically the two squirmer are not bond-aligned at the same time. The large value of $p \approx 0.6$ suggest that for a parallel alignment of $\boldsymbol{e}_2$ ($q_2 = 0$) with the bond, $\varphi_1 \approx 55^\circ$, and for the antiparallel alignment of $\boldsymbol{e}_1$ with the bond ($q_1 = -1$), $\varphi_2 \approx 125^\circ$, respectively (Fig. 2(d)). Hence, a coupled dynamics emerges, where squirmer pair switches from an antiparallel-oblique state of squirmer 1 and 2 to an oblique-parallel state and vice versa. This type of coupled alignments allows for a correlated rotational-type motion, which is reflected in the bond-vector autocorrelation function, Fig. 7, with its negative part.

The distribution functions for $\beta > 0$ are qualitatively similar with that for $\beta = 0$, they decay exponentially with maxima at $\cos\varphi = \pm 1$, corresponding to a preferred antiparallel alignment of the propulsion directions, and with widths decreasing with increasing β as shown in Fig. 8. The preferred orientation is illustrated in Fig. 2(a), (b) and explains the very low transport of neutral and puller squirmers.

We like to stress the importance of orientational fluctuations of the individual squirmers for the stability of the swimming motion. Although the PDFs of neutral squirmers show maxima at $\cos\varphi = \pm 1$, the averages $q \approx \pm 0.76$ (corresponding to $\pm 40^\circ$) are far from $q = \pm 1$, which significantly influences the transport properties of dumbbells.

4.3 Bond force

The preference in the alignment of the propulsion directions leads to a bond force,

$$F_b = k\,(|\boldsymbol{R}| - l)\,, \tag{13}$$

which depends on Péclet number and active stress. Figure 11 shows the bond force normalized by the Péclet number as a function of the active stress (see also Fig. S4 and S5). The bond force is positive for all Pe and β, hence, the squirmers repel each other. The difference between the force values for the various Pe are small, consistent with a nearly linear increase of F_b with Pe (Fig. S4). Neutral squirmers (and weak pullers at small Pe) exhibit the strongest repelling force due to the outward pointing antiparallel alignment of the propulsion directions (Fig. 11). With increasing active stress, $\beta > 0$, repulsion decreases and attraction is obtained for athermal pullers by their flow field characteristics[65].

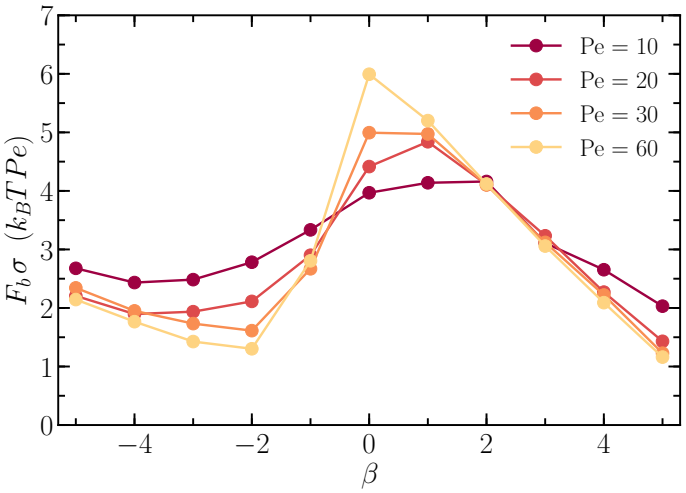

Fig. 11 Normalized bond force, F_b/Pe, as a function of the active stress, β, for the indicated Péclet numbers.

View Article Online
DOI: 10.1039/D0SM01569E

The latter is not the case for our thermal systems. Similarly, pushers show a reduced repulsion due to their preferred orientation roughly perpendicular to the bond vector. The repelling force increases again for strong pushers, because of the increasing probability of one of the propulsion directions to align with the bond.

As shown in Fig. S6, the bond force depends only weakly on the dumbbell bond length, l, for most active stresses, in particular for larger l, and for $l \to \infty$ an asymptotic values is assumed. Consistent with the simulation results, analytical calculations for ABP dumbbells[36] yield a bond force, which increases linearly with Péclet number (3) and is independent of the bond length. Even the magnitudes of the asymptotic forces are of the same order.

The presence of the bond has a major impact on the dumbbell overall flow field. The bond force on a squirmer gives rise to a Stokeslet by the coupling of the squirmer motion with the fluid as for a passive colloid, and by Newton's third law (action = reaction) the bond induces a "fluid" force dipole. The force-dipole strength $F_b l$ increases approximately linearly with the Péclet number (Fig. 11). Hence, depending on the squirmers active stress and the Péclet number, this dipolar flow field can dominate the squirming flow field. This is reflected by the flow fields displayed in Fig. 2.

4.4 Squirmer-squirmer propulsion alignment: dumbbell bond-length dependence

The flow field of a squirmer can be represented by a multipole expansion with contributions from the force dipole, the source dipole, the source quadrupole term, etc., which decay as $1/r^2$, $1/r^3$, $1/r^4$, and further terms of order $O(1/r^5)$, with the distance r from the squirmer center[11,91]. Hence, an increase of the dumbbell bond length, l, leads to a decrease of the flow field-mediated interactions, and in the asymptotic limit $l \to \infty$ the alignment parameter p (Eq. (10)) approaches zero. Interestingly, p of neutral squirmers changes only slowly over the considered range of bond lengths, as shown in Fig. 12 (cf. Fig. S3 for $\mathrm{Pe} = 10$), whereas

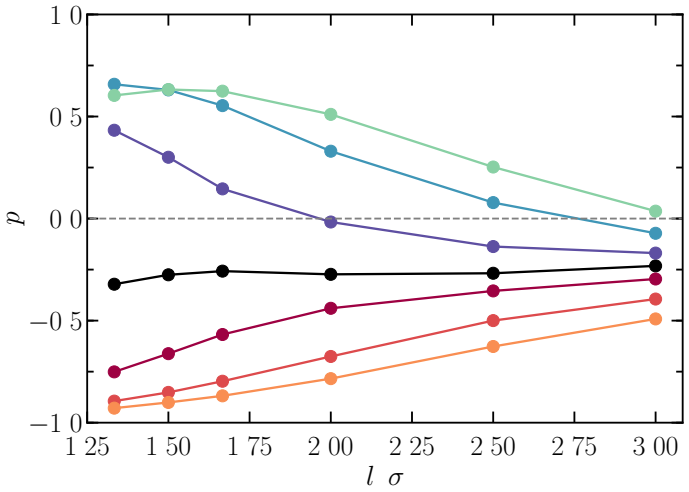

Fig. 12 Average alignment $p = \langle \boldsymbol{e}_1 \cdot \boldsymbol{e}_2 \rangle$ of the squirmer propulsion directions as a function of the dumbbell bond length for the active stress $\beta = 0, \pm 1, \pm 3$, and ± 5. The Péclet number is $\mathrm{Pe} = 30$. The color code is the same as in Fig. 3.

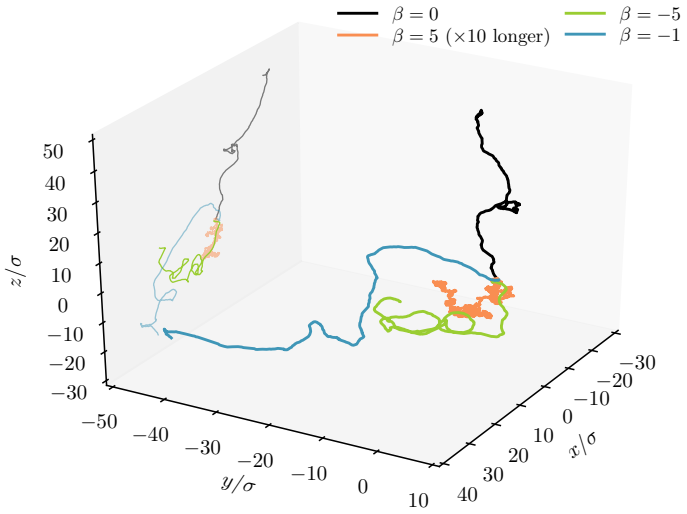

Fig. 13 Trajectories of the dumbbell center-of-mass for various active stresses β and $\mathrm{Pe} = 30$. Note that the trajectory for the center-of-mass position of the dumbbell with $\beta = 5$ is ten times longer. The lines on the left-hand side of the figure indicate projections of the trajectories in the xz plane.

$|p|$ of the curves for $\beta \neq 0$ decreases with increasing l. This can be explained by the force dipole generated by the bond, which evidently dominates the fluid-mediate interactions between the squirmers, since the interactions between the squirmer flow fields vanish with increasing l. Surprisingly, the curves for $\beta = -1$ and $\beta = -3$, maybe even for $\beta - 5$ at larger l, exhibit a non-monotonic behavior, crossing the $p = 0$ line and assume negative values before they approach the asymptotic value. Here, even for rather large bond lengths, the characteristics of the squirmer flow field matters.

5 Dumbbell dynamics

5.1 Squirmer trajectories and flow fields

Figure 13 shows characteristic trajectories of dumbbells for various active stresses. Evidently, they differ substantially qualitatively and quantitatively, in particular, the displacement of the pushers with $\beta = 5$ is very small compared to that of the neutral squirmers and weak pushers ($\beta = -1$). The latter is related to the antiparallel alignment of the propulsion directions along the bond. Trajectory of pushers with $\beta = -5$ exhibit circular parts, which emerge by the particular orientation of one of the squirmers pointing along the bond vector, as illustrated in Fig. 2(d).

The flow fields for the most probable squirmer geometries at the respective Péclet number are displayed Fig. 2. They are superpositions of the flow fields of the individual squirmers as well as the Stokeslet fields, generating a force dipole, emerging by to the bond force (cf. Sec. 4.3). Hence, the flow field is not strictly satisfying the boundary condition on the squirmers surface, nevertheless, it provides an impression of the actual field. Due to the bond-force fluid dipole, the velocity fields are predominantly dipolar, even for neutral squirmers. Yet, the near field is strongly dominated by the squirmer flow fields, which is particularly pronounced for strong pushers ($\beta = -5$) in Fig. 2(c) and 2(d).

View Article Online
DOI: 10.1039/D0SM01569E

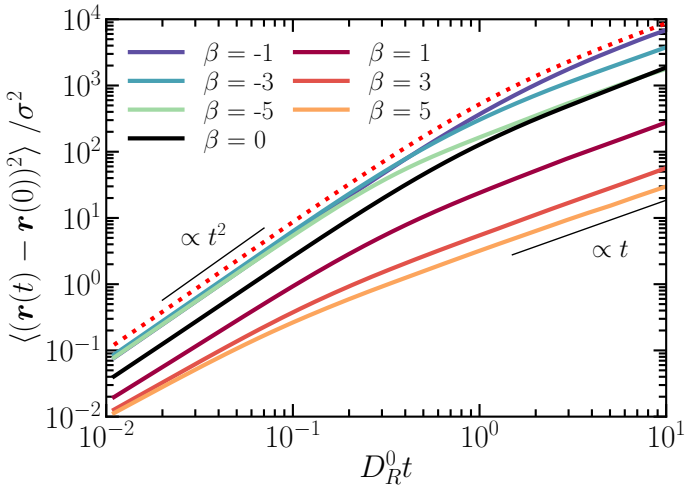

Fig. 14 Center-of-mass mean-square displacement of squirmer dumbbells as a function of the scaled time $D_R^0 t$ for the indicated active stresses and the Péclet number $\mathrm{Pe} = 30$. The red dotted line indicates the ABP dumbbell theoretical prediction Eq. (14) using the rotational diffusion coefficient, D_R^0, of an individual squirmer.

5.2 Center-of-mass mean-square displacement

The center-of-mass mean-square displacement (MSD) of dumbbells for various active stresses β is displayed in Fig. 14. The MSD shows two regimes that are characteristic of active particles. At short times $D_R^0 t \ll 1$, the dumbbells propagate ballistically with the MSD proportional to t^2, and for long times, $D_R^0 t \gg 1$, their motion is diffusive. Qualitatively, the dumbbell dynamics is described by the MSD of an active dumbbell of two ABPs[36],

$$\left\langle (\boldsymbol{r}_{\mathrm{cm}}(t) - \boldsymbol{r}_{\mathrm{cm}}(0))^2 \right\rangle = \frac{3k_B T}{\gamma_T} t + \frac{2v_0^2}{\gamma_R^2} \left(\gamma_R t + e^{-\gamma_R t} - 1 \right), \qquad (14)$$

with the translational diffusion coefficient $D_T^a = v_0^2/(6D_R) = \gamma_R/2$ of an individual ABP[36].

The strong dependence of the squirmer-dumbbell MSD on the active stress is illustrated in Fig. 14. In the ballistic regime, pushers with $-5 \leq \beta \leq -1$ exhibit an approximately active stress-independent displacement and swim velocity, as displayed in Fig. 15(a), where v is obtained by a fit of Eq. 14 (cf. Fig. S7 for examples of fits). The displacement decreases substantially for pullers with increasing β, and the dumbbell swim velocity becomes much smaller than the velocity v_0. Here too, for large $\beta > 0$, an active stress-independent velocity is assumed, which decreases with increasing Péclet number. Linked with the orientation of the propulsion directions, v changes substantially in the vicinity of $\beta = 0$ in a phase transition-like manner.

The crossover from the ballistic to diffusive motion shifts to shorter times with increasing magnitude of the active stress $|\beta| > 1$. As a consequence, for large $\beta \approx 5$, hardly any ballistic regime remains. At the same time, the diffusion coefficient decreases with increasing $|\beta| > 1$ and the respective dumbbell MSD can be even orders of magnitude smaller than that of ABP dumbbells. Quantitatively, the MSD of ABP dumbbells slightly overestimates that of pusher dumbbells with $\beta = -1$, which corresponds to a somewhat smaller swim velocity of squirmer dumbbells, but captures the time dependence well.

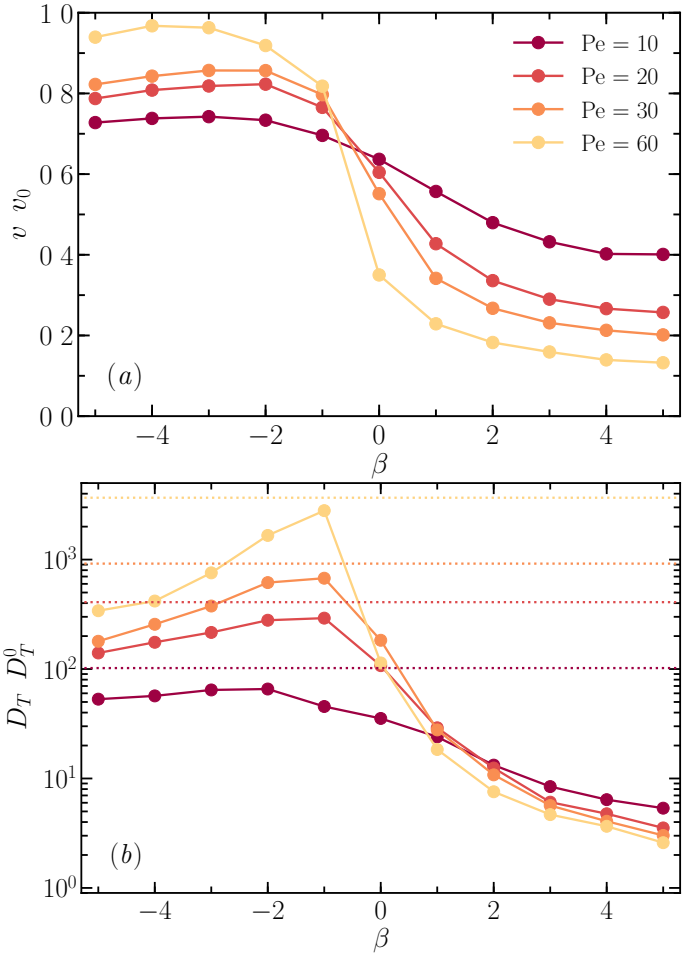

Fig. 15 (a) Effective swim velocity, v, and (b) center-of-mass active diffusion coefficient, D_T, of squirmer dumbbells as a function of the active stress, β, for the Péclet numbers $\mathrm{Pe} = 10$, 20, 30, and 60 (bottom to top at $\beta = -5$). The horizontal dotted lines indicate the diffusion coefficients of ABP dumbbells.

Figure 15(b) depicts the diffusion coefficients for various β and Péclet numbers. There is a substantial quantitative difference between the D_T values of pushers and pullers, where pusher dumbbells diffuse always faster than dumbbells of neutral squirmers and pullers. For pushers ($\beta \leq -1$), D_T increases monotonically with increasing Pe, but it is always smaller than the D_T of ABP dumbbells. For neutral squirmers and weak pullers ($\beta < 2$), D_T can change non-monotonically as a function of Pe. The change of D_T in the vicinity of $\beta = 0$ is substantial, rather abrupt, and increases with increasing activity. This suggests a jump, phase transition-like, change of the squirmer dynamics in the range $-2 < \beta < 2$ for asymptotically large Pe, since D_T increases, e.g., for $\beta = -1$, and decreases simultaneously for, e.g., $\beta = 1$ with increasing Pe.

The substantial qualitative different diffusive behavior of the various dumbbells is related the preferred alignment of the squirmers' propulsion direction. The outward-oriented antiparallel alignment along the bond of pullers ($\beta > 0$) naturally leads to a cancellation of the propulsion and no stable swimming is

View Article Online
DOI: 10.1039/D0SM01569E

obtained for athermal dumbbell pullers[65], which corresponds to the limit $\mathrm{Pe} \to \infty$ in our case. However, thermal fluctuations perturb the perfect alignment, and a finite active transport is obtained with a diffusion coefficient larger than the thermal value for $\mathrm{Pe} < \infty$. Even more, the alignment of pushers gives rise to strong active transport. As a consequence, stable and fast swimming of such dumbbells is obtained.

6 Summary and conclusions

To elucidate the effect of thermal fluctuations and internal hydrodynamic interactions on the transport properties of microswimmers, we have performed mesoscale hydrodynamics simulations of active dumbbells composed of linked squirmers with geometrically unrestricted rotational motion. We find a strong influence of the squirmers' flow fields on their rotational dynamics, stationary-state orientation of the propulsion directions with respect to each other and the bond vector, and their swimming behavior.

Squirmers in dumbbells exhibit a faster decay of the autocorrelation function of the propulsion direction for $\beta < -1$ and $\beta \gtrsim 3$ than independent squirmers by the coupling of the squirmer flow fields and the fluid force dipole emerging from the bond. Specifically for pushers, the effect is amplified with increasing Péclet number. For the range $-1 < \beta < 3$, the relaxation time increases with increasing Pe. The relaxation times of the crosscorrelation function, τ_c, of the propulsion directions are typically longer than those of the autocorrelation function, τ_s, of individual squirmers and the Brownian relaxation time, $1/\gamma_R$, of ABPs. Mainly for strong pushers and large Pe, τ_c values are assumed, which are smaller than those of ABP dumbbells.

The hydrodynamic coupling of the squirmer flow fields leads to a preferred stationary-state alignment of their propulsion directions. The propulsion directions of pushers with $-5 < \beta < -1$ are nearly parallel and orient approximately normal to the bond vector, with larger fluctuations of the latter. Pullers ($\beta > 0$) align in an antiparallel manner with respect to each other and along the dumbbell bond vector. The source-dipole flow field of neutral squirmers ($\beta = 0$) is sufficient to produce a weak antiparallel coupling. The average cosine, $p = \langle \cos\vartheta \rangle$, of the angle between the propulsion directions exhibits a rapid change in the vicinity of $\beta = 0$, which becomes sharper with increasing Pe, and is reminiscent of a transition from a preferred parallel alignment of the $\boldsymbol{e}_i$ for $\beta < 0$ to an antiparallel alignment for $\beta > 0$. Noteworthy, we find two bistable orientational states for strong pusher dumbbells ($\beta = -5$), where the squirmer pairs fluctuate between states of oblique-parallel or oblique-antiparallel alignment of the two propulsion directions, which slows down the overall directed motion compared to weak pushers. Such states lead to a (short time) rotational motion of the dumbbell as reflected in circular trajectories.

The preferred alignment of the propulsion directions substantially affects the dumbbell motility. In particular the activity-dominated diffusion coefficient, D_T, of pullers decreases with increasing β and for large Pe is only a factor $2-3$ larger than the thermal diffusion coefficient. In contrast, the diffusion coefficient of pushers dumbbells is orders of magnitudes larger, in particular for $\beta \approx -1$. However, D_T is in always smaller than that of ABP dumbbells. As the alignment, D_T changes very rapidly in the vicinity of $\beta = 0$ from a very large value ($\beta < 0$) to a value close to D_T^0 ($\beta > 0$) of passive dumbbells. Since D_T of ABP dumbbells grows as Pe^2 with increasing Péclet number, we can expect an even stronger jump-like behavior of D_T in the limit $\mathrm{Pe} \gg 1$.

Our simulations reflect aspects predicted theoretically for athermal squirmer dumbbells within the far-field approximation[65], in particular, the low swimming ability of pullers due to the preferred stable antiparallel orientation of the squirmer propulsion directions. However, in strong contrast to the theoretical predictions for athermal systems, pushers exhibit a large active transport. For $\beta \approx -1$, the diffusion coefficient D_T is even close to that of ABP dumbbells. This difference reflects the importance of thermal fluctuations and near-field hydrodynamic effects on the transport properties of squirmer assemblies. Hence, fluid flow could be a factor, which mediates assembling and collective swimming of microorganisms in polymeric structures observed in some planktonic species[92,93].

Our simulation studies reveal a strong influence of microswimmer flow fields on the motility of dumbbells. Similarity, for linear polymer-like assemblies, it has been show that the hydrodynamic coupling between monomer flow fields gives rise to intricate motion patters, such as rotation or beating, even in absence of swimming[94]. The effect of these flow fields on the swimming properties of longer polymer-like structures remains to be elucidated.

ABP dumbbell systems exhibit motility-induced phase separation[37,50]. Considering the major impact of the squirmer flow fields on the dumbbell dynamics and the alignment of their propulsion directions, we expect also pronounced effects on the dumbbell phase behavior. As has been shown for spheres and spheroids, the squirmer flow field can substantially modify the phase behavior, from a suppression of MIPS for spheres to an enhanced phase separation for spheroids in 2D[60]. A hydrodynamically restricted rotational freedom of the individual squirmers may give rise to a distinctly different phase behavior or/and collective dynamics. Studies of such systems are under way.

Our studies clearly reveal that tuning the squirmers' flow fields provides means to control the swimming behavior of dumbbells. This flexibility is a fundamental prerequisite for the rational design of synthetic microswimmer assemblies based on pusher-/puller-type active units for future autonomous microbot applications.

Conflicts of interest

There are no conflicts to declare.

Acknowledgements

The support of this work from the DFG priority program SPP 1726 "Microswimmers - from Single Particle Motion to Collective Behaviour" is gratefully acknowledged. The authors gratefully acknowledge the computing time granted through JARA-HPC on the supercomputer JURECA at Forschungszentrum Jülich.

Notes and references

1 M. E. Cates and J. Tailleur, *EPL*, 2013, **101**, 20010.

View Article Online
DOI: 10.1039/D0SM01569E

2 A. P. Solon, M. E. Cates and J. Tailleur, *Eur. Phys. J. Spec. Top.*, 2015, **224**, 1231.
3 J. Elgeti, R. G. Winkler and G. Gompper, *Rep. Prog. Phys.*, 2015, **78**, 056601.
4 C. Bechinger, R. D. Leonardo, H. Löwen, C. Reichhardt, G. Volpe and G. Volpe, *Rev. Mod. Phys.*, 2016, **88**, 1 – 50.
5 G. Gompper, R. G. Winkler, T. Speck, A. Solon, C. Nardini, F. Peruani, H. Löwen, R. Golestanian, U. B. Kaupp, L. Alvarez, T. Kiørboe, E. Lauga, W. C. K. Poon, A. DeSimone, S. Muiños-Landin, A. Fischer, N. A. Söker, F. Cichos, R. Kapral, P. Gaspard, M. Ripoll, F. Sagues, A. Doostmohammadi, J. M. Yeomans, I. S. Aranson, C. Bechinger, H. Stark, C. K. Hemelrijk, F. J. Nedelec, T. Sarkar, T. Aryaksama, M. Lacroix, G. Duclos, V. Yashunsky, P. Silberzan, M. Arroyo and S. Kale, *J. Phys: Condens. Matter*, 2020, **32**, 193001.
6 A. P. Berke, L. Turner, H. C. Berg and E. Lauga, *Phys. Rev. Lett.*, 2008, **101**, 038102.
7 J. Elgeti and G. Gompper, *EPL*, 2013, **101**, 48003.
8 Y. Fily, A. Baskaran and M. F. Hagan, *Soft Matter*, 2014, **10**, 5609.
9 U. Marini Bettolo Marconi and C. Maggi, *Soft Matter*, 2015, **11**, 8768.
10 S. Das, G. Gompper and R. G. Winkler, *New J. Phys.*, 2018, **20**, 015001.
11 M. Theers, E. Westphal, G. Gompper and R. G. Winkler, *Soft Matter*, 2016, **12**, 7372 – 7385.
12 H. H. Wensink, J. Dunkel, S. Heidenreich, K. Drescher, R. E. Goldstein, H. Löwen and J. M. Yeomans, *Proc. Natl. Acad. Sci. USA*, 2012, **109**, 14308.
13 A. Sokolov and I. S. Aranson, *Phys. Rev. Lett.*, 2012, **109**, 248109.
14 A. Cavagna and I. Giardina, *Annu. Rev. Condens. Matter Phys.*, 2014, **5**, 183.
15 G. Popkin, *Nature*, 2016, **529**, 16.
16 A. Be'er and G. Ariel, *Mov. Ecol.*, 2019, **7**, 9.
17 G. K. Auer, P. M. Oliver, M. Rajendram, T.-Y. Lin, Q. Yao, G. J. Jensen and D. B. Weibel, *mBio*, 2019, **10**, e00210–19.
18 H. Li, X.-q. Shi, M. Huang, X. Chen, M. Xiao, C. Liu, H. Chaté and H. P. Zhang, *Proc. Natl. Acad. Sci. USA*, 2019, **116**, 777.
19 H. Chaté, *Annu. Rev. Condens. Matter Phys.*, 2020, **11**, 189.
20 M. E. Cates and F. C. MacKintosh, *Soft Matter*, 2011, **7**, 3050.
21 D. Needleman and Z. Dogic, *Nat. Rev. Mater.*, 2017, **2**, 17048.
22 A. Martín-Gómez, T. Eisenstecken, G. Gompper and R. G. Winkler, *Soft Matter*, 2019, **15**, 3957.
23 R. G. Winkler and G. Gompper, *J. Chem. Phys.*, 2020, **153**, 040901.
24 J. R. Howse, R. A. L. Jones, A. J. Ryan, T. Gough, R. Vafabakhsh and R. Golestanian, *Phys. Rev. Lett.*, 2007, **99**, 048102.
25 M. C. Marchetti, Y. Fily, S. Henkes, A. Patch and D. Yllanes, *Curr. Opin. Colloid Interface Sci.*, 2016, **21**, 34.
26 P. Romanczuk, M. Bär, W. Ebeling, B. Lindner and L. Schimansky-Geier, *Eur. Phys. J. Spec. Top.*, 2012, **202**, 1.
27 A. Zöttl and H. Stark, *J. Phys.: Condens. Matter*, 2016, **28**, 253001.
28 M. R. Shaebani, A. Wysocki, R. G. Winkler, G. Gompper and H. Rieger, *Nat. Rev. Phys.*, 2020, **2**, 181.
29 F. Peruani, A. Deutsch and M. Bär, *Phys. Rev. E*, 2006, **74**, 030904.
30 Y. Fily and M. C. Marchetti, *Phys. Rev. Lett.*, 2012, **108**, 235702.
31 J. Bialké, T. Speck and H. Löwen, *Phys. Rev. Lett.*, 2012, **108**, 168301.
32 G. S. Redner, M. F. Hagan and A. Baskaran, *Phys. Rev. Lett.*, 2013, **110**, 055701.
33 A. Wysocki, R. G. Winkler and G. Gompper, *EPL*, 2014, **105**, 48004.
34 J. Stenhammar, D. Marenduzzo, R. J. Allen and M. E. Cates, *Soft Matter*, 2014, **10**, 1489 – 1499.
35 P. Digregorio, D. Levis, A. Suma, L. F. Cugliandolo, G. Gonnella and I. Pagonabarraga, *Phys. Rev. Lett.*, 2018, **121**, 098003.
36 R. G. Winkler, *Soft Matter*, 2016, **12**, 3737 – 3749.
37 J. T. Siebert, J. Letz, T. Speck and P. Virnau, *Soft Matter*, 2017, **13**, 1020.
38 A. Ghosh and N. S. Gov, *Biophys. J.*, 2014, **107**, 1065.
39 A. Kaiser, S. Babel, B. ten Hagen, C. von Ferber and H. Löwen, *J. Chem. Phys.*, 2015, **142**, 124905.
40 H. Vandebroek and C. Vanderzande, *Phys. Rev. E*, 2015, **92**, 060601.
41 D. Osmanovic and Y. Rabin, *Soft Matter*, 2017, **13**, 963.
42 T. Eisenstecken, G. Gompper and R. G. Winkler, *Polymers*, 2016, **8**, 304.
43 R. G. Winkler, J. Elgeti and G. Gompper, *J. Phys. Soc. Jpn.*, 2017, **86**, 101014.
44 S. M. Mousavi, G. Gompper and R. G. Winkler, *J. Chem. Phys.*, 2019, **150**, 064913.
45 A. Suma, G. Gonnella, D. Marenduzzo and E. Orlandini, *EPL*, 2014, **108**, 56004.
46 L. F. Cugliandolo, P. Digregorio, G. Gonnella and A. Suma, *Phys. Rev. Lett.*, 2017, **119**, 268002.
47 L. F. Cugliandolo, G. Gonnella and A. Suma, *Phys. Rev. E*, 2015, **91**, 062124.
48 S. Ebbens, R. A. L. Jones, A. J. Ryan, R. Golestanian and J. R. Howse, *Phys. Rev. E*, 2010, **82**, 015304.
49 A. Nourhani, S. J. Ebbens, J. G. Gibbs and P. E. Lammert, *Phys. Rev. E*, 2016, **94**, 030601.
50 P. Digregorio, D. Levis, A. Suma, L. F. Cugliandolo, G. Gonnella and I. Pagonabarraga, *J. Phys.: Conf. Ser.*, 2019, **1163**, 012073.
51 M. J. Lighthill, *Commun. Pure Appl. Math.*, 1952, **5**, 109 – 118.
52 J. Blake, *J. Fluid Mech.*, 1971, **46**, 199 – 208.
53 I. Llopis and I. Pagonabarraga, *J. Non-Newtonian Fluid Mech.*, 2010, **165**, 946 – 952.
54 T. Ishikawa, M. P. Simmonds and T. J. Pedley, *J. Fluid Mech.*, 2006, **568**, 119 – 160.

View Article Online
DOI: 10.1039/D0SM01569E

55 I. O. Götze and G. Gompper, *Phys. Rev. E*, 2010, **82**, 1 – 9.

56 J. J. Molina, Y. Nakayama and R. Yamamoto, *Soft Matter*, 2013, **9**, 4923.

57 M. Kuron, P. Stärk, C. Burkard, J. de Graaf and C. Holm, *J. Chem. Phys.*, 2019, **150**, 144110.

58 G. Gompper, T. Ihle, D. M. Kroll and R. G. Winkler, *Advanced Computer Simulation Approaches for Soft Matter Sciences III*, ed. P. C. Holm and P. K. Kremer, Springer, Berlin, Heidelberg, 2009, pp. 1 – 87.

59 W. E. Uspal, M. N. Popescu, S. Dietrich and M. Tasinkevych, *Soft Matter*, 2015, **11**, 6613.

60 M. Theers, E. Westphal, K. Qi, R. G. Winkler and G. Gompper, *Soft Matter*, 2018, **14**, 8590 – 8603.

61 T. Ishikawa and M. Hota, *The Journal of Experimental Biology*, 2006, **209**, 4452 – 4463.

62 R. Matas-Navarro, R. Golestanian, T. B. Liverpool and S. M. Fielding, *Phys. Rev. E*, 2014, **90**, 032304.

63 N. Yoshinaga and T. B. Liverpool, *Phys. Rev. E*, 2017, **96**, 020603.

64 Z. Shen, A. Würger and J. S. Lintuvuori, *Soft Matter*, 2019, **15**, 1508.

65 T. Ishikawa, *Micromachines*, 2019, **10**, 1 – 16.

66 A. Malevanets and R. Kapral, *J. Chem. Phys.*, 1999, **110**, 8605 – 8613.

67 R. Kapral, *Adv. Chem. Phys.*, 2008, **140**, 89–146.

68 Y.-G. Tao and R. Kapral, *J. Chem. Phys.*, 2008, **128**, 164518.

69 M. T. Downton and H. Stark, *J. Phys.: Condens. Matter*, 2009, **21**, 1 – 6.

70 A. Zöttl and H. Stark, *Phys. Rev. Lett.*, 2014, **112**, 1 – 5.

71 R. G. Winkler and G. Gompper, *Handbook of Materials Modelling: Hydrodynamics in motile active matter*, Springer Nature, 2018, pp. 1 – 21.

72 A. Zöttl and H. Stark, *Eur. Phys. J. E*, 2018, **41**, 61.

73 K. Qi, E. Westphal, G. Gompper and R. G. Winkler, *Phys. Rev. Lett.*, 2020, **124**, 068001.

74 K. Qi, H. Annepu, G. Gompper and R. G. Winkler, *Phys. Rev. Research*, 2020, **2**, 033275.

75 R. Pöhnl, M. N. Popescu and W. E. Uspal, *J. Phys: Condens. Matter*, 2020, **32**, 164001.

76 A. P. Solon, J. Stenhammar, R. Wittkowski, M. Kardar, Y. Kafri, M. E. Cates, and J. Tailleur, *Phys. Rev. Lett.*, 2015, **10**, 1 – 6.

77 H. Noguchi and G. Gompper, *Phys. Rev. E: Stat. Nonlinear, Soft Matter Phys.*, 2008, **78**, 016706.

78 M. Theers and R. G. Winkler, *Phys. Rev. E: Stat. Nonlinear, Soft Matter Phys.*, 2015, **91**, 033309.

79 C.-C. Huang, A. Chatterji, G. Sutmann, G. Gompper and R. G. Winkler, *J. Comput. Phys.*, 2010, **229**, 168.

80 E. Westphal, S. P. Singh, C.-C. Huang, G. Gompper and R. G. Winkler, *Comput. Phys. Commun.*, 2014, **185**, 495 – 503.

81 I. P. Omelyan, *Phys. Rev. E*, 1998, **58**, 1169.

82 A. Lamura, G. Gompper, T. Ihle and D. M. Kroll, *Europhys. Lett.*, 2001, **56**, 319 – 325.

83 J. T. Padding, A. Wysocki, H. Löwen and A. A. Louis, *J. Phys. Condens. Matter*, 2005, **17**, S3393.

84 M. Theers and R. G. Winkler, *Soft Matter*, 2014, **10**, 5894.

85 E. Lauga, *Soft Matter*, 2011, **7**, 3060.

86 L. D. Favro, *Phys. Rev.*, 1960, **119**, 53 – 62.

87 R. G. Winkler, A. Wysocki and G. Gompper, *Soft Matter*, 2015, **11**, 6680 – 6691.

88 S. Tavaddod, M. A. Charsooghi, F. Abdi, H. R. Khalesifard and R. Golestanian, *Eur. Phys. J. E*, 2011, **34**, 1.

89 K. Drescher, J. Dunkel, L. H. Cisneros, S. Ganguly and R. E. Goldstein, *Proc. Natl. Acad. Sci. USA*, 2011, **108**, 10940.

90 The diffusion coefficient D_R^0 differs from that of a rigid dumbbell by a factor 3/2, because the flexible dumbbell includes fluctuations along the bond.

91 S. E. Spagnolie and E. Lauga, *J. Fluid Mech.*, 2012, **700**, 105.

92 M. H. Sohn, K. W. Seo, Y. S. Choi, S. J. Lee, Y. S. Kang and Y. S. Kang, *Mar. Biol.*, 2011, **158**, 561 – 570.

93 S. Lovecchio, E. Climent, R. Stocker and W. M. Durham, *Sci. Adv.*, 2019, **5**, 1 – 9.

94 A. Laskar and R. Adhikari, *Soft Matter*, 2015, **11**, 9073.